http://dx.doi.org/10.14500/aro.11948

Optimizing a Compact Ring Coupler with Neural Network Modeling for Enhanced Performance in Radio Frequency Applications

Sobhan Roshani[1], Salah I. Yahya[2,3], Bita Najafi[4], Ali Jadidian[4], Mohsen Karimi[1] and Saeed Roshani[1†]

[1]Department of Electrical Engineering, Ker.C., Islamic Azad University, Kermanshah, Iran

[2]Department of Software Engineering, Faculty of Engineering, Koya University, Koya 46017, F.R. - Iraq

[3]Department of Computer Technology Engineering, College of Technical Engineering, Al-Hadba University, Mosul, F.R. - Iraq

[4]Department of Computer Engineering, Ker.C., Islamic Azad University, Kermanshah, Iran

Abstract*—This paper presents the design and optimization of a compact 900 MHz hybrid ring coupler using lumped reactive components, aimed at achieving harmonic suppression and size reduction for Radio Frequency (RF) applications. Traditional hybrid ring couplers rely on quarter-wavelength transmission lines, resulting in large size device and limited harmonic rejection. To address these challenges, a novel coupler structure was developed that replaces long transmission lines with composite branches, significantly reducing device dimensions while enhancing performance. In the proposed coupler, instead of the six conventional 90-degree lines, six compact networks composed of microstrip lines, three inductors, and one capacitor are used. The inductors have values of L_1, L_1, L_2, and the capacitor has a value of C. These four parameters significantly influence the coupler's performance; thus, they were selected as inputs for the applied neural network, with the scattering parameters S_{11}, S_{12}, S_{13}, S_{14}, and frequency considered as the five output parameters. The dielectric constant (ε_r) of the substrate is 2.2, and the substrate material is RT/duroid 5880 with a thickness of 20 mils. By feeding the neural network model with these parameters as inputs, the coupler's output response was predicted and analyzed, enabling the selection of optimal component values. Optimal responses were obtained with L_1 = 10.1 nH, L_2 = 2.3 nH and C = 2.1 pF, which allows the coupler to operate effectively at 900 MHz. At this operating frequency, the values are S_{11} = −32.6 dB, S_{12} = −3.05 dB, S_{13} = −3.03 dB, and S_{14} = −45.9 dB, indicating excellent coupler performance.

***Index Terms* – Coupler, Harmonic suppression, Neural network, Size reduction**

ARO-The Scientific Journal of Koya University
Vol. XIII, No.1(2025), Article ID: ARO.11948. 9 pages
DOI: 10.14500/aro.11948
Received: 13 December 2024; Accepted: 31 March 2025
Regular research paper; Published: 11 April 2025
†Corresponding author's e-mail: s.roshani@iau.ir

I. Introduction

Microwave couplers, such as branch-line couplers, directional couplers, rat-race couplers, and other types, which split and combine signals with equal amplitude are widely used in modern wireless systems (Rezaei, et al., 2023). Conventional couplers occupy a large area; for example, branch-line and rat-race couplers consist of four and six long quarter-wavelength ($\lambda/4$) transmission lines, respectively, which results in significant large area consumption. This large size is undesirable for modern communication systems (Venter, et al., 2018). Furthermore, conventional couplers suffer from presence of unwanted harmonics in frequency response, which cause undesirable non-linear effects in overall system (Nikandish, et al., 2020).

In the past decade, several solutions have been provided to miniaturize the large size of conventional couplers and suppress unwanted harmonics. The applied reactive components (L and C) in the structure of microwave couplers are an effective method to reduce circuit size and filter signals at unwanted frequency ranges (Jamshidi, et al., 2021).

In (Du, et al., 2018) capacitors were used to provide a miniaturized hybrid coupler with wide suppression band. In some works (Beigizadeh, et al., 2017) applied lumped-element in a hybrid coupler which results in a narrow operating bandwidth, which should be considered in coupler design.

Applied electromagnetic bandgap (EBG) cell in the structure of microwave coupler is another effective method to reduce circuit size and filter signals at unwanted frequency ranges, but EBG cells need extra fabrication process and increase the design complexity of the coupler which is undesirable (Lin, et al., 2007; Ooi, 2005).

Furthermore, using open-ended stubs, different types of resonators and filters are common methods widely used in coupler structures to eliminate unwanted harmonics

(Mohammadi, et al., 2024; Mezaal, et al., 2024; Roshani, et al., 2023b; Roshani, et al., 2023a; Al-Majdi and Mezaal, 2023). For example, in (Roshani, et al., 2022a), open-ended stubs are used in a microwave coupler, which provides an 80% size reduction and suppresses second to sixth harmonics. However, in many designs using open stubs and resonators lead to complex structures which are undesirable.

In (Long, et al., 2024) circular-shaped resonators were used to design a compact coupler with harmonic suppression. This coupler is designed for medical imaging systems and achieves an 80% size reduction and suppresses second to fifth harmonics.

The presented study in (Wang, et al., 2007) shows how using slow-wave structures in microstrip branch-line couplers can decrease the required area to just 28% of the size of a traditional design at 2.0 GHz, while also effectively suppressing second harmonics. However, designing slow-wave structures can be challenging, as their performance varies based on substrate material and thickness. In another study introduced in (Yang, et al., 2012), adding open-circuit stubs at the center and ends of each branch-line section helps reduce size and control harmonics. However, these stubs can introduce unwanted side effects and need careful manufacturing to work properly. In (Mirzavand, et al., 2012) inductors and two-section branches are used to design a compact power divider which has a wide harmonics suppression band. This divider has complex structure.

The 900 MHz frequency is commonly used in many wireless communication systems, such as mobile phones, Wi-Fi networks, and Internet of Things devices. It falls within the Ultra High Frequency band and is ideal for long-range communication because it can travel over longer distances and through obstacles, such as walls. This makes it a popular choice for communication technologies that require reliable signals over a wide area. In addition, 900 MHz is often used for low-power devices, as it offers a good balance between signal strength and energy efficiency. In this study, the 900 MHz frequency is chosen because it is widely used in various Radio Frequency (RF) applications, making it relevant for real-world use and ensuring that the designed coupler can meet the needs of these systems.

In this work, an ultra-compact ring coupler using lumped inductors and capacitors is designed at 900 MHz. The proposed coupler achieves a 99% size reduction and provides a wide suppression band from 1.8 GHz to 10 GHz. In the proposed coupler design a neural network model is used to obtain the best values of the applied lumped inductors and capacitors to achieve great performance of scattering parameters.

II. Conventional 900 MHz Ring Coupler Design

The structure of the conventional 900 MHz Rat Race Coupler (RRC) is shown in Fig. 1. This coupler consists of six uniform quarter-wavelength (λ/4) transmission lines, with a $\sqrt{2}Z_0$ (70.7 Ω) characteristic impedance. An RT/duroid

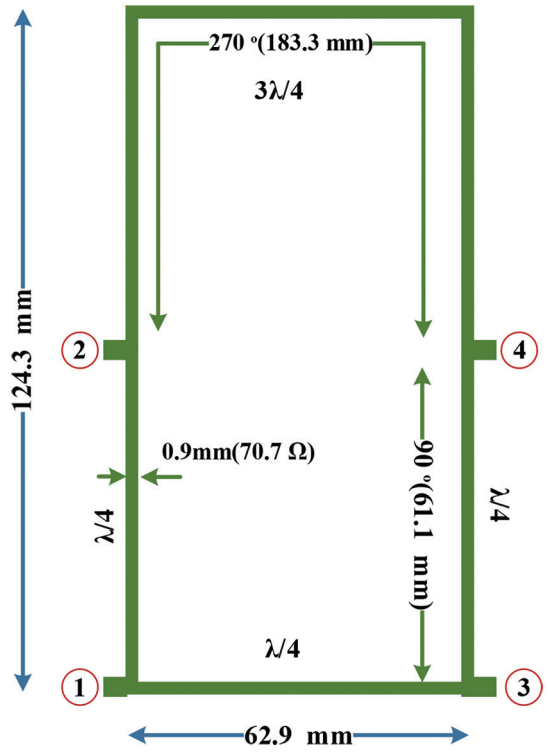

Fig. 1. The structure of the conventional rat race coupler operating at a frequency of 900 MHz.

substrate with a 20-mil thickness and a dielectric constant of 2.2 is used, with each branch having a length of 61.1 mm and a width of 0.9 mm. The overall size of the conventional 900 MHz RRC is 124.3 mm × 62.9 mm (0.50λ × 0.25λ).

The scattering parameters of the conventional RRC are depicted in Fig. 2. As shown, the coupler operates effectively at 900 MHz, achieving an input return loss and port isolation exceeding 51 dB and 50 dB, respectively. The insertion losses for the other ports are well within an acceptable range, with $S_{12} = S_{13} = -3.1$ dB.

III. Proposed Transmission Line using Lumped Components

In Fig. 3, the conventional transmission line branch used in the conventional RRC design at 900 MHz is depicted. Fig. 3a shows the layout of a conventional λ/4 transmission line branch, which has long size of 61.1 mm. Fig. 3b illustrates the frequency response of this conventional branch, indicating its performance at the target frequency of 900 MHz. At the operating frequency of 900 MHz, S_{12} is approximately −0.54 dB, and S_{11} is −9.7 dB, indicating that the conventional $\lambda/4$ transmission line effectively passes the signal at 900 MHz.

In Fig. 4, the proposed transmission line branch for the RRC is presented. This branch utilizes a modified design with lumped components to reduce its size while achieving the same performance at 900 MHz. Fig. 4a presents the layout of the proposed branch, which occupies less physical space compared to the conventional branch. In the proposed line

http://dx.doi.org/10.14500/aro.11948

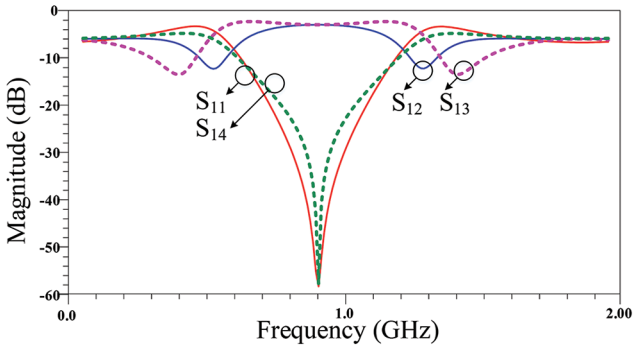

Fig. 2. Scattering parameters of the conventional rat race coupler at an operating frequency of 900 MHz.

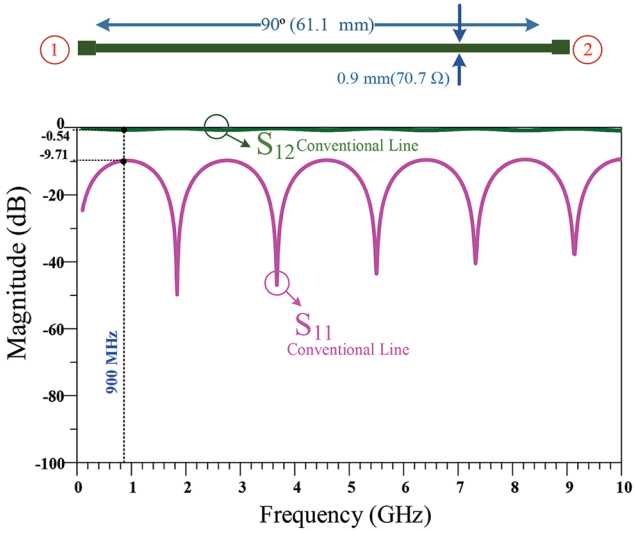

Fig. 3. Conventional λ/4 transmission line: (a) layout, and (b) frequency response at 900 MHz.

L_1 = 10.1 nH, L_2 = 2.3 nH and C = 2.1 pF. Fig. 4b displays the frequency response of the proposed branch, showing that it not only matches the performance of the conventional branch at 900 MHz but also provides harmonic suppression at higher frequencies, making it more effective for compact and high-performance coupler designs. At the operating frequency of 900 MHz, S_{12} is approximately −0.55 dB, and S_{11} is −9.6 dB, indicating that the proposed transmission line effectively passes the signal at 900 MHz.

IV. Proposed Lumped Element Structure

The structure of the proposed 900 MHz RRC is shown in Fig. 5. In this structure, six proposed transmission lines are used instead of the six long λ/4 branches. Each proposed line has one capacitor and three inductors. These lumped components (L_1, L_1, L_2, and C) have a significant effect on the coupler performance. To improve the performance of the coupler and find the best values of these components a neural network model is used. These values of L_1, L_2, and C were used as inputs for the neural network model and scattering

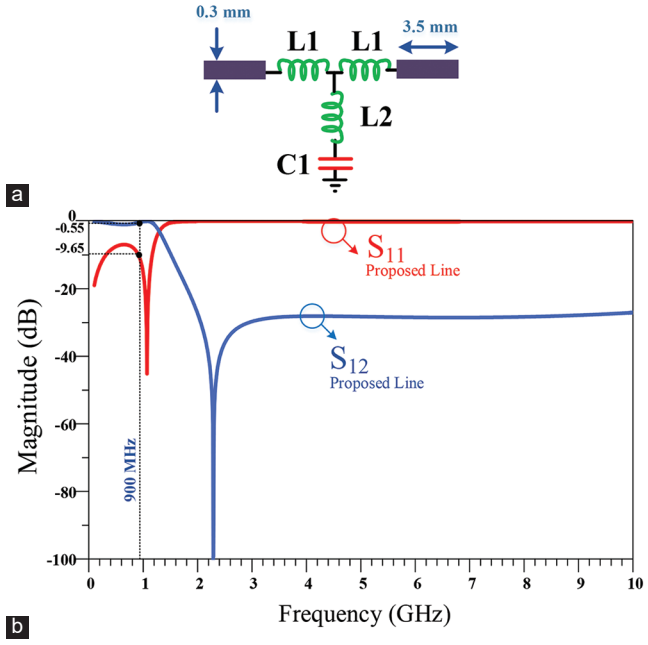

Fig. 4. Structure of the (a) proposed 900 MHz transmission line and (b) its frequency response.

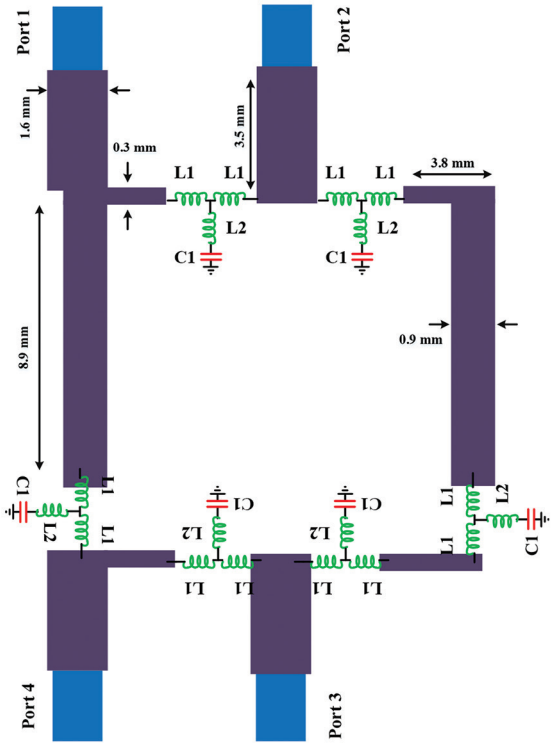

Fig. 5. Structure of the proposed 900 MHz rat race coupler.

parameters of S_{11}, S_{12}, S_{13}, S_{14}, and the frequency response were defined as the five outputs of the neural network model. The neural network was used to find the optimal values of the lumped components.

Fig. 5 illustrates the structure of the proposed RRC, designed to operate at 0.9 GHz. This coupler consists of

six proposed transmission lines, each incorporating three inductors and one capacitor. The inductors are labeled as L_1, L_1, and L_2, and the capacitor is labeled as C. To improve the performance of the coupler, the values of the lumped components (L_1, L_1, L_2, and C), which are crucial to the coupler function, were used as inputs for a neural network model. This model provides outputs of the scattering parameters (S_{11}, S_{12}, S_{13}, and S_{14}) and the frequency response, helping to adjust the component values for better performance. In the next steps, the neural network was used to find the optimal values for these components, ensuring the coupler performs as desired at 0.9 GHz.

V. Proposed Artificial Neural Network

The Long Short-Term Memory (LSTM) neural network model is used in this paper to predict the desired parameters. The LSTM is a special and improved type of recurrent neural network (RNN), which is suitable for the designed microwave coupler. The LSTM consists of memory cells for storing information, and gates to control and manage the flow of information. The input gates enter new data into memory cells, while the forget gates decide, which information should be deleted. Furthermore, the output gates decide how much of the stored information will be passed to the final output.

Fig. 6 depicts the flowchart of using the proposed LSTM model to predict the scattering parameters. As explained in the flow chart, the process begins with data preparation, followed by training the LSTM model on the dataset. Finally, the trained model is used to make accurate predictions for the proposed RRC.

The training process for the LSTM model starts with preparing the dataset by normalizing the data using a technique called MinMaxScaler, which ensures that the values are in a range suitable for the neural network to process. After the data are prepared, the LSTM model is trained using this dataset. The model has multiple layers, including an input layer, LSTM layers, and a final layer that makes predictions. The LSTM layers help the model understand patterns in the data over time. During training, the optimizer is used to adjust the learning process and reduce errors, which are measured using a method called Mean Squared Error (MSE). The model is also validated with a separate set of data that wasn't used in training to see how well it can generalize to new data. After the training, the model is tested using a new set of data, and its predictions are compared to the real values. Finally, the predicted values are adjusted back to their original scale, and the model's performance is checked using two metrics: MSE and Mean Relative Error (MRE), to see how accurate the model is at predicting the desired outcomes.

A. Dataset Analysis

The dataset of this study contains electromagnetic (EM) simulations of the proposed structure for the RRC. The input parameters are L_1 (nH), L_2 (nH), and C (pF), while the output ones are considered to be the scattering parameters and the main frequency, which are S_{11} (dB), S_{12} (dB), S_{13} (dB), S_{14} (dB), and frequency (MHz). The total of 60 sample is used to form the dataset as listed in Table I. Furthermore, the real values of the output parameters are given in this table. The simulation data is provided using advanced design system (ADS) software.

The dataset shown in Table I are generated through EM simulations conducted 60 times, each with different dimensions for the components of the RRC. These simulations were carried out using ADS software, which is commonly used for modeling and analyzing RF components. The input parameters for each simulation included the values

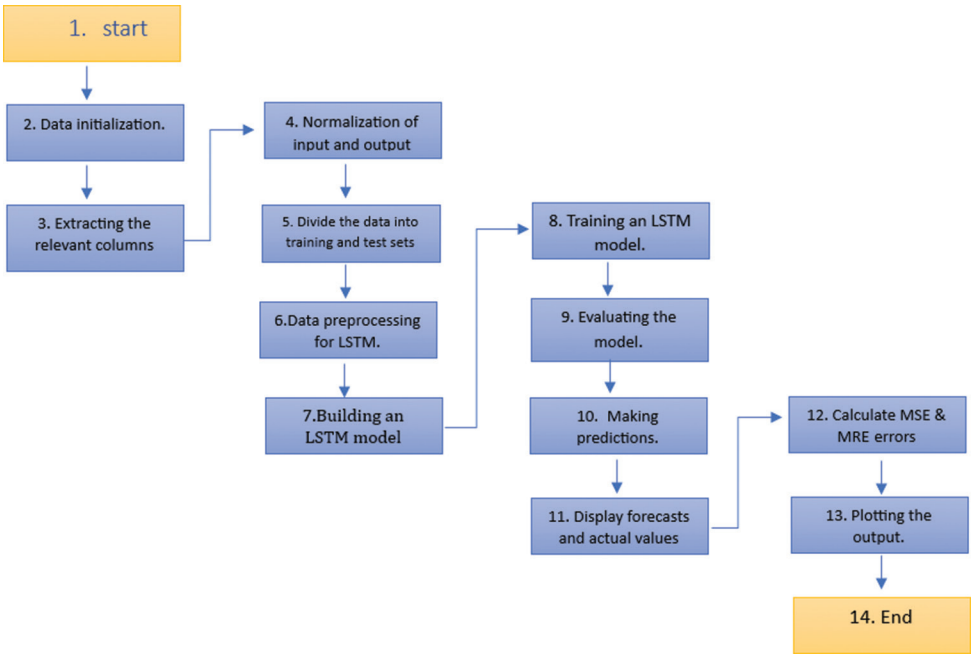

Fig. 6. Flowchart of using the proposed long short-term memory model.

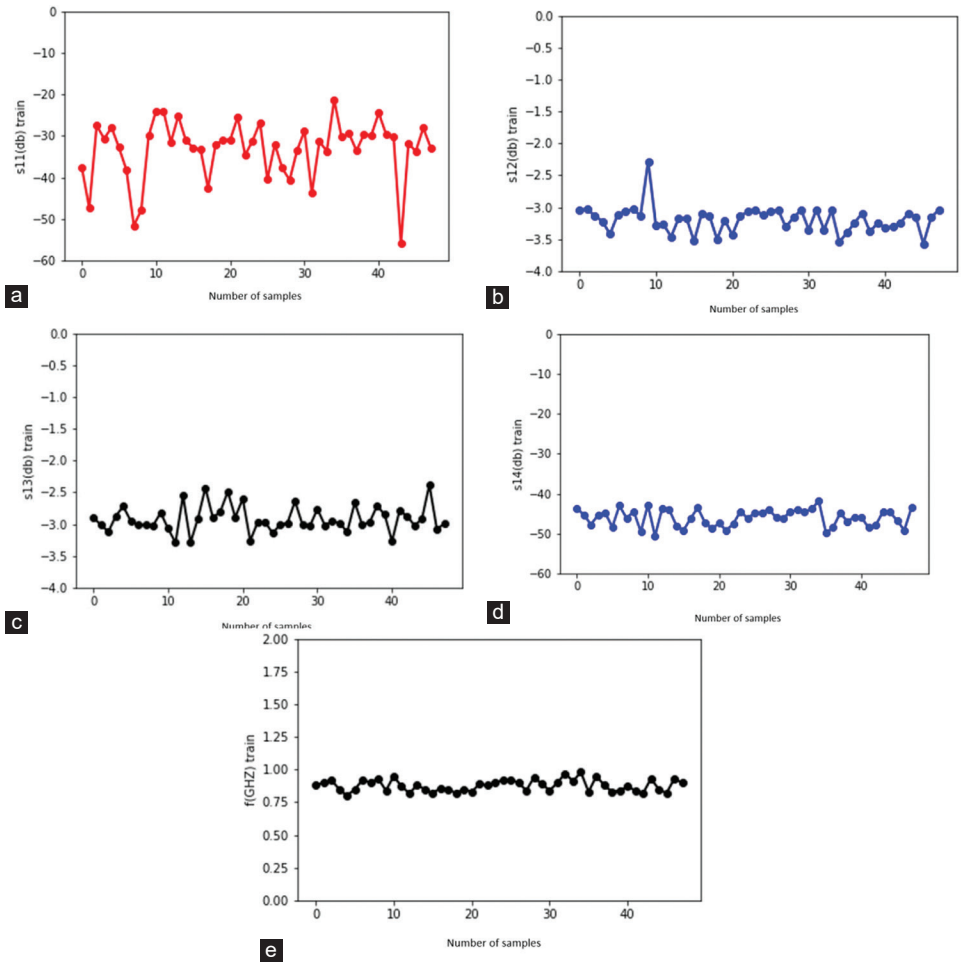

Fig. 7. The proposed ANN training results. Training performance of the proposed long short-term memory for (a) S_{11}, (b) S_{12}, (c) S_{13}, (d) S_{14}, and (e) f (GHz) parameters.

for L_1 (nH), L_2 (nH), and C (pF), while the output parameters were the scattering parameters (S_{11}, S_{12}, S_{13}, S_{14}) in dB, along with the main frequency in GHz. Each row in Table I corresponds to a different simulation run, with unique values for the input parameters and the corresponding output results. This provides a diverse set of data that was used to train and test the neural network model.

B. Applied LSTM RNN Method

The LSTM model is used to predict the parameters of the proposed coupler using the Keras and TensorFlow libraries. The MinMaxScaler function is used to normalize data before processing for better results. Then, data are divided into training and testing phases using the train_test_split function. The LSTM layer is built using 50 units for processing sequential data. The ReLU activation function is used in the model to understand the non-linear behavior of the data. Furthermore, a dense layer consisting of 5 units and a linear activation function is added for better prediction. Then, the Adam optimizer is used for adjusting the learning rate. The MSE and MRE metrics are used for reducing the difference between the predicted and actual values. In the training phase, the mode is run for 1000 epochs with a batch size of 10 and validation is executed using test data.

The results of the proposed ANN LSTM model at the training level are illustrated in Fig. 7. The plots show that the proposed model accurately predicts the values, indicating successful training. Furthermore, it can be concluded that the proposed model has predicted various parameters accurately in different ranges.

In Fig. 7a, the S_{11} training data are shown, which represents how much of the signal is reflected back at port 1. Fig. 7b shows the S_{12} training data, which represents the transmission loss from port 1 to port 2. In Fig. 7c, the S_{13} training data are presented, showing the transmission loss from port 1 to port 3. Fig. 7d illustrates the S_{14} training data, which represents the isolation between ports 1 and 4. Fig. 7e shows the frequency training data.

Furthermore, the results of the proposed ANN LSTM model at the test level are illustrated in Fig. 8. The plots in the sub figures show that the proposed model has perfectly predicted the values in the test phase. Furthermore, it can be concluded that the proposed model has predicted unseen data accurately.

Fig. 8a presents the S_{11} test data, which indicates how much of the signal is reflected back at port 1. Fig. 8b shows the S_{12} test data, representing the transmission loss from port 1 to port 2. Fig. 8c illustrates the S_{13} test data, which shows the

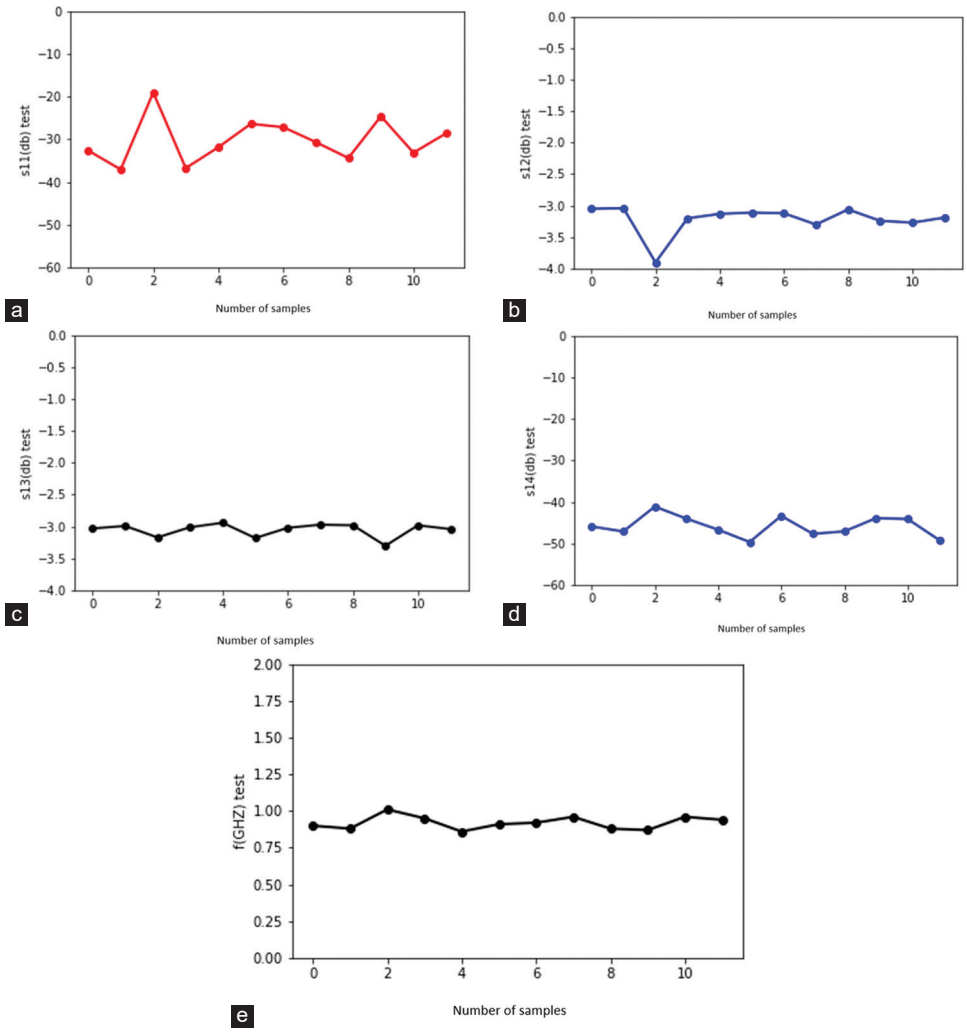

Fig. 8. The proposed ANN test results. Test performance of the proposed long short-term memory for (a) S_{11}, (b) S_{12}, (c) S_{13}, (d) S_{14}, and (e) f (GHz) parameters.

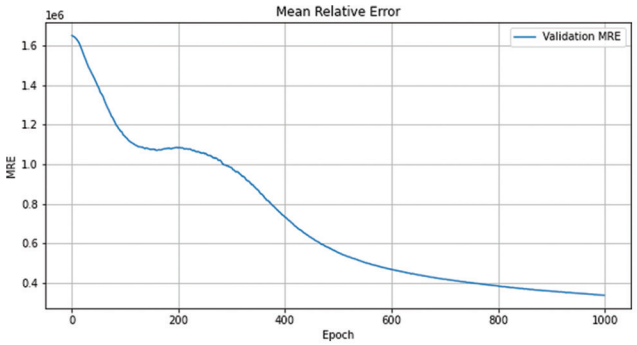

Fig. 9. Values of MRE over different epochs for the proposed ANN long short-term memory model.

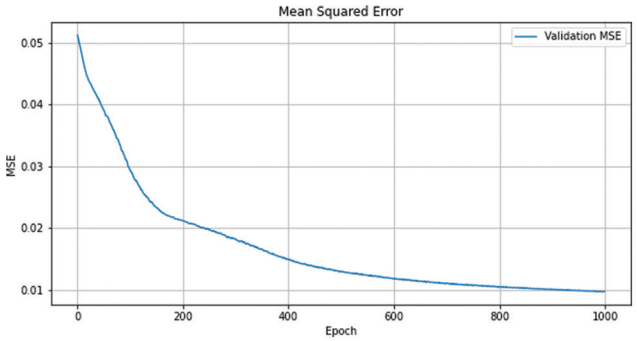

Fig. 10. Values of MSE over different epochs for the proposed ANN long short-term memory model.

transmission loss from port 1 to port 3. Fig. 8d displays the S_{14} test data, representing the isolation between ports 1 and 4. Finally, Fig. 8e presents the frequency test data, showing how well the model predicts the frequency based on the test set.

The MRE and MSE metrics are utilized to analyze the proposed ANN model results. The MRE and MSE metrics are written in Equations (1) and (2). In these equations, the *actual* and *predicted* indices indicate the real and predicted data.

$$\text{MRE} = \frac{1}{n}\sum_{i=1}^{n}\frac{\left|y_{pred} - y_{actual}\right|}{y_{actual} + \varepsilon} \quad (1)$$

$$\text{MRE} = \frac{1}{n}\sum_{i=1}^{n}\left(y_{pred} - y_{actual}\right)^2 \quad (2)$$

http://dx.doi.org/10.14500/aro.11948

TABLE I
APPLIED DATASET FOR THE TRAINING AND TESTING PHASES OF THE NEURAL NETWORK

Input parameters			Output parameters				
L_1 (nH)	L_2 (nH)	C_1 (pF)	S_{11} (dB)	S_{12} (dB)	S_{13} (dB)	S_{14} (dB)	f (MHz)
10.2	2.3	2.1	33.5	3.04	3.03	46.2	890
10.3	2.3	2.1	43.78	3.04	3.02	44.1	900
10.4	2.3	2.1	47.4	3.03	3.01	45.3	900
10.5	2.3	2.1	51.6	3.03	3.01	46.14	900
10.5	2.3	2.2	37.1	3.04	2.99	47.13	880
10.5	2.3	2.3	32.8	3.12	2.95	48.4	850
10.5	2.3	2.4	30.1	3.24	2.87	47.9	820
10.5	2.3	2.5	28	3.42	2.72	44.83	800
10.5	2.2	2.3	33.3	3.1	2.9	46.2	860
10.5	2.1	2.3	33.6	3.09	2.97	44.9	880
10.5	2	2.3	34.6	3.07	2.97	47.5	880
10.5	1.9	2.3	34.4	3.06	2.98	47.1	880
10.5	2.4	2.3	31.9	3.13	2.94	46.7	860
10.5	2.5	2.3	31.9	3.15	2.92	44.65	850
10.5	2.6	2.3	31.1	3.17	2.91	48	850
10.5	2.7	2.3	31.02	3.2	2.89	48.8	850
10.5	2.8	2.3	30.7	3.22	2.87	45.4	850
10.5	2.9	2.3	29.9	3.25	2.85	45.9	840
10.5	3	2.3	30.06	2.28	2.82	49.52	840
10.5	3.1	2.3	29.65	3.31	2.79	48.53	840
10.5	3.2	2.3	28.8	3.35	2.76	44.5	840
10.6	3.2	2.3	29.7	3.38	2.71	46.9	830
10.7	3.2	2.3	30.3	3.4	2.66	49.85	830
10.8	3.2	2.3	30.93	3.43	2.6	47.4	830
10.9	3.2	2.3	31.58	3.46	2.55	43.7	820
11	3.2	2.3	32.25	3.5	2.49	47.23	820
11.1	3.2	2.3	32.9	3.53	2.43	49.2	820
11.2	3.2	2.3	33.7	3.57	2.38	46.76	820
11.2	3.2	2.2	37.77	3.31	2.64	44.08	840
11.2	3.2	2.1	42.56	3.13	2.8	43.5	850
11.2	3.2	2	37.69	3.04	2.9	43.69	880
11.2	3.2	1.9	31.22	3.04	2.97	44.46	900
11.2	3.2	1.8	27.19	3.12	3.02	43.36	920
11.2	3.2	1.7	24	3.28	3.07	42.85	950
11.2	3.2	1.6	21.36	3.54	3.12	41.87	980
11.2	3.2	1.5	19.07	3.9	3.17	41.15	1010
11.1	3.2	1.9	32.02	3.04	2.98	44.72	900
11	3.2	1.9	32.83	3.04	2.99	43.57	900
10.9	3.2	1.9	33.65	3.05	2.99	43.82	910
10.6	3.2	1.9	38.19	3.06	3.01	43.01	920
10.5	3.2	1.9	40.39	3.07	3.01	44.83	920
10.2	3.2	1.9	55.86	3.1	3.02	44.5	930
10	3.2	1.9	47.89	3.13	3.02	44.45	930
9.8	3.2	1.9	40.66	3.16	3.01	45.94	940
9.6	3.2	1.9	36.76	3.2	3.01	44.03	950
9.3	3.2	1.9	33.16	3.27	2.98	44.13	960
9	3.2	1.9	31.4	3.35	2.95	44.57	970
9	3.4	1.9	30.7	3.3	2.97	47.71	960
9	3.7	1.9	29.47	3.24	3.01	48.5	950
9	4	1.9	28.66	3.19	3.04	49.2	940
9	4.3	1.9	28.11	3.16	3.08	49.17	930
9	4.6	1.9	27.54	3.13	3.12	47.73	920
9	4.8	1.9	26.76	3.12	3.14	46.21	920
9	5.1	1.9	26.4	3.11	3.18	49.67	910
9	5.7	1.9	25.5	3.14	3.26	49.29	890
9	6	1.9	25.2	3.17	3.29	44.02	880
9	6.4	1.9	24.64	3.24	3.3	43.91	870
9	6.5	1.9	24.11	3.27	3.29	50.6	870
9	6.7	1.9	24.52	3.32	3.27	46.05	870

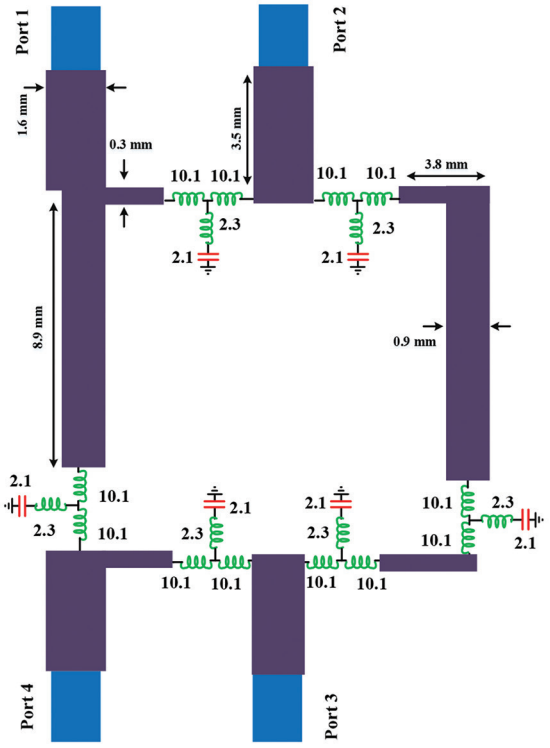

Fig. 11. Layout of the proposed rat race coupler. The inductors and capacitors are in nH and pF units.

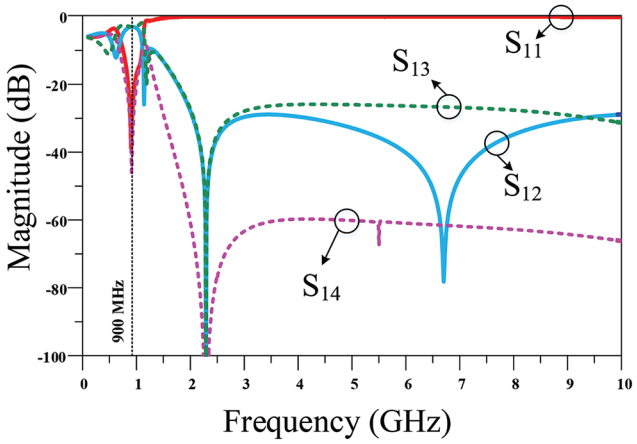

Fig. 12. Simulated frequency response of the designed rate race coupler.

The values of calculated MRE and MSE over different epochs for the proposed ANN LSTM model are shown in Figs. 9 and 10, respectively. The decreasing values of MRE and MSE over epochs demonstrate that the proposed model is well trained and can predict data accurately. After training, the data are denormalized using MinMaxScaler for improved interpretation. The final values of MSE and MRE are calculated as 0.0108 and 0.0663, proving the accuracy of the proposed model.

VI. PROPOSED COUPLER CONFIGURATION

According to the proposed neural network, the best performance of the coupler can be achieved by the following values of inductors and capacitors: L_1 = 10.1 nH, L_2 = 2.3

TABLE II
PERFORMANCE COMPARISON OF COUPLER DESIGNS FOCUSED ON SIZE REDUCTION AND HARMONIC SUPPRESSION

References	Design approach	Operating frequency (MHz)	Size reduction (%)	Harmonic suppression band (GHz)	Key features
(Pozar, 2012)	Conventional λ/4 coupler	900	0	None	Simple structure, large size
(Du, et al., 2018)	Lumped components-based	559	83.5	1.1–2.8	Compact design, limited suppression
(Lin, et al., 2007)	EBG structure	2400	34.5	7.2–12	Moderate suppression, complex to fabricate
(Ooi, 2005)	EBG resonator	2500	0	10–14	Enhanced suppression, increased cost
(Jamshidi, et al., 2021)	Wilkinson power divider (Lumped components)	800	82.8	1.6–20	High suppression
(Coromina, et al., 2020)	Non-periodic step impedance shunt stubs	1000	67.7	2–10	Moderate suppression, and size reduction
(Lalbakhsh, et al., 2021)	Open-ended stubs	1800	74	3.6–12.6	Simple structure
(Roshani, et al., 2022b)	Resonators	750	84	1.5–5.25	Compact size
This work	Proposed ANN-optimized design	900	99	1.8–10	Ultra-compact, excellent suppression

nH, and C = 2.1 pF. The layout of the proposed RRC is illustrated in Fig. 11. The layout of the proposed structure occupies only 10.9 mm × 6.7 mm, featuring a 99% size reduction compared to the conventional coupler.

Fig. 12 depicts the simulated frequency response of the designed rate race coupler operating at 900 MHz. The obtained return loss (S_{11}) and isolation (S_{14}) are 39.1 dB and 45.6 dB. Furthermore, the achieved insertion losses at port 2 (S_{12}) and port 3 (S_{13}) are 3.05 dB and 3.07 dB, respectively. The obtained harmonic suppression band ranges from 1.8 GHz to 10 GHz, in which the unwanted harmonics are suppressed with high attenuation.

A performance comparison of the proposed coupler with other related works, focused on the size reduction and harmonic suppression, is presented in Table II. As shown, the proposed RRC has obtained excellent size reduction of 99% and desirable harmonic suppression, which outperforms other related works in terms of miniaturization and harmonic suppression.

VII. Conclusion

A new RRC is presented in this paper with excellent size reduction operating at 900 MHz. Lumped elements are applied in this structure and the proposed design is optimized using a neural network. The final size of the designed coupler is 10.9 mm × 6.7 mm, which shows a 99% size reduction compared to the conventional coupler with a size of 124.3 mm × 62.9 mm. The best values of the applied lumped components are determined using the proposed neural network, resulting in an improved performance of the device. The proposed coupler also demonstrates excellent harmonic suppression from 1.8 GHz to 10 GHz, which results in better performance and prevents the presence of unwanted spurious harmonics in the frequency response. The obtained desirable results show that the proposed RRC can be considered as a strong candidate for use in modern communication systems.

References

Al-Majdi, K., and Mezaal, Y.S., 2023. New miniature narrow band microstrip diplexer for recent wireless communications. *Electronics*, 12(3), pp.716.

Beigizadeh, M., Dehghani, R., and Nabavi, A., 2017. Analysis and design of a lumped-element hybrid coupler using limited quality factor of components. *AEU-International Journal of Electronics and Communications*, 82, pp.312-320.

Coromina, J., Velez, P., Bonache, J., and Martín, F., 2020. Branch line couplers with small size and harmonic suppression based on non-periodic step impedance shunt stub (SISS) loaded lines. *IEEE Access*, 8, pp.67310-67320.

Du, R.N., Weng, Z.B., and Zhang, C., 2018. A miniaturized filtering 3-dB branch-line hybrid coupler with wide suppression band. *Progress in Electromagnetics Research Letters*, 73, pp.83-89.

Jamshidi, M.B., Roshani, S., Talla, J., Roshani, S., and Peroutka, Z., 2021. Size reduction and performance improvement of a microstrip Wilkinson power divider using a hybrid design technique. *Scientific Reports*, 11(1), pp.7773.

Lalbakhsh, A., Mohamadpour, G., Roshani, S., Ami, M., Roshani, S., Sayem, A.S.M., Alibakhshikenari, M., and Koziel, S., 2021. Design of a compact planar transmission line for miniaturized rat-race coupler with harmonics suppression. *IEEE Access*, 9, pp.129207-129217.

Lin, C.M., Su, H.H., Chiu, J.C., and Wang, Y.H., 2007. Wilkinson power divider using microstrip EBG cells for the suppression of harmonics. *IEEE Microwave and Wireless Components Letters*, 17(10), pp.700-702.

Long, Z., Zhang, B., Liu, G., Wu, Z., and Yan, Q., 2024. A compact branch-line coupler with harmonic suppression using novel circular-shaped resonators for medical imaging systems. *Multiscale and Multidisciplinary Modeling, Experiments and Design*, 7, pp.1-18.

Mezaal, Y.S., Ghazi, H.S., and Khaleel, M.H., 2024. Highly narrowband miniaturized microstrip diplexer for qubit mobile communication networks utilizing SIR and T-shaped resonators with negative group delay performance. *Optical and Quantum Electronics,* 56, pp.1670.

Mirzavand, R., Honari, M.M., Abdipour, A., and Moradi, G., 2012. Compact microstrip Wilkinson power dividers with harmonic suppression and arbitrary power division ratios. *IEEE Transactions on Microwave Theory and Techniques*, 61(1), pp.61-68.

Mohammadi, N., Moloudian, G., Roshani, S., Roshani, S., Parandin, F., and Lalbakhsh, A., 2024 A Wilkinson power divider with harmonic suppression through low-pass filter for GSM and LTE applications. *Scientific Reports*, 14(1), pp.2429.

Nikandish, G., Staszewski, R.B., and Zhu, A., 2020. Breaking the bandwidth limit: A review of broadband Doherty power amplifier design for 5G. *IEEE Microwave Magazine*, 21(4), pp.57-75.

Ooi, B.L., 2005. Compact EBG in-phase hybrid-ring equal power divider. *IEEE Transactions on Microwave Theory and Techniques,* 53(7), pp.2329-2334.

Pozar, D.M., 2012. *Microwave Engineering*. 4th ed. University of Massachusetts at Amherst, John Wiley and Sons, Inc, United States, pp.26-30.

Rezaei, A., Yahya, S.I., and Nouri, L., 2023. A comprehensive review on microstrip couplers. *Aro-The Scientific Journal Of Koya University*, 11(1), pp.22-31.

Roshani, S., Koziel, S., Yahya, S.I., Chaudhary, M.A., Ghadi, Y.Y., Roshani, S., and Golunski, L., 2023a. Mutual coupling reduction in antenna arrays using artificial intelligence approach and inverse neural network surrogates. *Sensors*, 23(16), pp.7089.

Roshani, S., Yahya, S., Roshani, S., Farahmand, A., and Hemmati, S., 2022a. Design of a modified compact coupler with unwanted harmonics suppression for L-band applications. *Electronics*, 11, p.1747.

Roshani, S., Yahya, S.I., Mezaal, Y.S., Chaudhary, M.A., Al-Hilali, A.A., Mojirleilani, A., and Roshani, S., 2023b. Design of a compact quad-channel microstrip diplexer for L and S band applications. *Micromachines* (*Basel*), 14(3), pp.553.

Roshani, S., Yahya, S.I., Roshani, S., and Rostami, M., 2022b. Design and fabrication of a compact branch-line coupler using resonators with wide harmonics suppression band. *Electronics*, 11(5), pp.793.

Venter, J.J., Stander, T., and Ferrari, P., 2018, X-band reflection-type phase shifters using coupled-line couplers on single-layer RF PCB. *IEEE Microwave and Wireless Components Letters*, 28(9), pp.807-809.

Wang, J., Wang, B.Z., Guo, Y.X., Ong, L., and Xiao, S., 2007. A compact slow-wave microstrip branch-line coupler with high performance. *IEEE Microwave and Wireless Components Letters*, 17(7), pp.501-503.

Yang, G., Li, B., Kang, W., and Ge, S., 2012. Miniaturized microstrip branch-line coupler with good harmonic suppression performance. *Journal of Electronics (China)*, 29(1), pp.132-136.